

U-FaceBP: Uncertainty-aware Bayesian Ensemble Deep Learning for Face Video-based Blood Pressure Measurement

Yusuke Akamatsu[†], Terumi Umematsu, Hitoshi Imaoka
 NEC Corporation, Japan
[†]yusuke-akamatsu@nec.com

Abstract

Blood pressure (BP) measurement plays an essential role in assessing health on a daily basis. Remote photoplethysmography (rPPG), which extracts pulse waves from camera-captured face videos, has the potential to easily measure BP for daily health monitoring. However, there are many uncertainties in BP estimation using rPPG, resulting in limited estimation performance. In this paper, we propose U-FaceBP, an uncertainty-aware Bayesian ensemble deep learning method for face video-based BP measurement. U-FaceBP models three types of uncertainty, *i.e.*, data, model, and ensemble uncertainties, in face video-based BP estimation with a Bayesian neural network (BNN). We also design U-FaceBP as an ensemble method, with which BP is estimated from rPPG signals, PPG signals estimated from face videos, and face images using multiple BNNs. A large-scale experiment with 786 subjects demonstrates that U-FaceBP outperforms state-of-the-art BP estimation methods. We also show that the uncertainties estimated from U-FaceBP are reasonable and useful for prediction confidence.

1. Introduction

Blood pressure (BP) is an important vital sign of human health status. According to the World Health Organization (WHO) [52], the number of adults with high BP (*i.e.*, hypertension) has reached 1.28 billion. Hypertension increases the risk of heart, brain, and kidney disease. It is estimated that 30-50% of hypertensive patients are unaware of their own disease [43], so daily BP monitoring is essential. Mercury or electronic sphygmomanometers are commonly used for BP measurement, in which a cuff wrapped around the arm is compressed to measure the pressure exerted by blood. However, compression by the cuff is uncomfortable for users and inconvenient for continuous BP monitoring.

Electrocardiogram (ECG)- and photoplethysmography (PPG)-based methods have been investigated as cuffless BP measurement methods. These methods can be divided

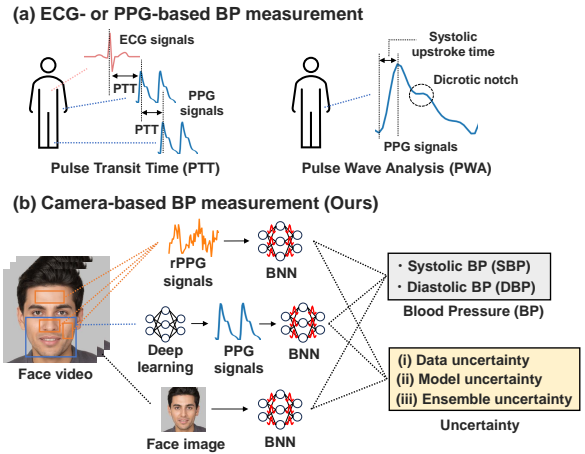


Figure 1. (a) PTT- and PWA-based methods for cuffless BP measurement using ECG or PPG. (b) Our U-FaceBP for camera-based BP measurement. We design U-FaceBP as an ensemble method consisting of rPPG signals, PPG signals (estimated from face videos), and face image-based BP estimation models. U-FaceBP outputs predicted BP and its uncertainty.

into two main categories (see Fig. 1 (a)): pulse transit time (PTT) [6, 10, 24, 29, 75]- and pulse wave analysis (PWA) [33, 35, 61, 65, 74]-based methods. Based on the fact that PTT and BP are negatively correlated [23], ECG and PPG or multiple PPG sensors are used to calculate PTT, and estimate BP. However, it is necessary to attach two sensors to different parts of the body (*e.g.*, chest and fingertips, toes and fingertips [6]) to calculate PTT, which is inconvenient for users. PWA-based methods require only one PPG sensor because BP is estimated by analyzing the PPG waveform (*e.g.*, systolic upstroke time and dicotic notch shown in Fig. 1 (a)) are related to BP). Nevertheless, since PPG sensors are not widely available in homes and are contact-based devices, they are not suitable for daily BP measurement.

In recent years, BP measurement from camera-captured face videos has attracted attention as an alternative to using PPG sensors [19, 46]. This approach is very promising for daily BP monitoring because it uses commonly

available webcams and smartphones and is a non-contact measurement approach. The basic principle of BP estimation from face videos is the analysis of pulse waves extracted from the videos, called remote PPG (rPPG) signals [36, 42, 44, 59, 60, 66, 71, 72, 77]. Another approach involves extracting multiple rPPG signals from different parts of the face (*e.g.*, cheeks and forehead) and uses the PTT features derived from these rPPG signals to estimate BP [55, 72, 73]. Several methods [72, 73] use not only rPPG signals but also age and body mass index (BMI) estimated from face images, which are related to BP [17, 54].

Although BP measurement from face videos is promising, several factors make BP estimation challenging. First, rPPG is a subtle signal and sensitive to noise due to body motion and lighting environment, which can easily degrade BP estimation performance [66]. It has also been reported that pulse wave features are related to BP, but the validity of BP estimation from pulse waves remains low [47]. Furthermore, the cardiovascular system is highly individualized, and the performance of BP estimation from rPPG signals depends on the person [60]. Therefore, there are many uncertainties in BP estimation from face videos, resulting in limited estimation performance.

In this paper, we propose an uncertainty-aware Bayesian ensemble deep learning method for face video-based BP measurement called *U-FaceBP* (see Fig. 1 (b)). *U-FaceBP* models the uncertainty in face video-based BP estimation with a Bayesian neural network (BNN). Unlike a standard neural network (NN), a BNN can account for uncertainty in deep learning [30]. *U-FaceBP* is also an ensemble method for estimating BP using multiple BNNs to incorporate various BP-related features. *U-FaceBP* handles the following three types of uncertainty: (i) data (aleatoric) uncertainty: noise inherent in the observations, such as uncertainty of BP estimation from pulse waves and individual differences in the cardiovascular system; (ii) model (epistemic) uncertainty: indicating a lack of knowledge of the model, and unknown data for which the NN has not been trained have a high uncertainty; and (iii) ensemble uncertainty: representing the confidence from multiple model predictions, a large variance in predictions across models indicates a high uncertainty. By focusing on these three uncertainties, we calculate the confidence in the predicted BPs. We can leverage confidence in real-world applications, such as accepting confident predictions and re-measuring with a sphygmomanometer for unconfident predictions.

In the ensemble method, we construct models from three different perspectives for face video-based BP estimation. The first is BP estimation using rPPG signals. We extract multiple rPPG signals from different facial parts and estimate BP by using both pulse waveform and PTT features. The second is BP estimation using PPG signals estimated from the face video. Although rPPG signals are

extracted from face videos on the basis of signal processing approaches (*e.g.*, green signal [68] and plane-orthogonal-to-skin (POS) [69]), such hand-crafted features are noisy, and the quality of pulse waves may be low. We estimate PPG signals (acquired from a contact-type PPG sensor) from face videos on the basis of deep learning and precisely extract the pulse waveform. The third is BP estimation from face images. To incorporate facial appearance information (*e.g.*, facial shape [4, 62], wrinkles, and baldness [37, 41] related to hypertension) other than age and BMI [72, 73], we estimate BP directly from face images. The predictions from the three perspectives, *i.e.*, rPPG signals, PPG signals (estimated from face videos), and face images, are integrated into a final predicted BP.

We conduct an experiment involving a large-scale dataset created from 786 subjects, focusing on the pitfalls [47] of the experimental setting in BP estimation. Specifically, we ensure that a wide range of BPs are included in the dataset and that subjects for model training and testing do not overlap. The experimental results indicate that *U-FaceBP* achieves significantly better BP estimation performance than state-of-the-art (SoTA) BP estimation methods. The main contributions of this paper are;

- *U-FaceBP* is the first uncertainty-aware face video-based BP estimation method. We confirm that incorporating uncertainty improves BP estimation performance and that there is a relationship between calculated prediction confidence and BP estimation performance.
- We propose the novel ensemble BP estimation method using rPPG signals, PPG signals estimated from face videos, and face images. Compared to previous BP estimation approaches that rely on rPPG signals, our approach significantly improves estimation performance.
- We conduct an experiment with a large dataset from 786 subjects for face video-based BP measurement. We evaluate the performance for practical use scenarios, such as avoiding overlapping subjects in the training and test data.

2. Related Work

Face Video-based Blood Pressure Measurement: Face video-based physiological measurements (*e.g.*, heart rate and respiratory rate) have made great advancements in the last 15 years [13, 58, 69]. This technology, known as rPPG or image PPG (iPPG), extracts pulse waves from videos by capturing subtle changes in reflected light on the skin. The rPPG technique has the potential to estimate the essential vital sign of blood pressure (BP), and the number of papers on face video-based BP estimation has increased in recent years [19, 46]. Luo *et al.* [44] were the first to investigate BP estimation from face videos on a large dataset. They extracted rPPG signals via transdermal optical imaging then estimated BP using multilayer perceptron. However, additional meta-features, including room temper-

ature and an individual’s physical characteristics (*e.g.*, age, weight, and skin tone), are required to be input into the model. Schrumph *et al.* [60] trained a convolutional neural network (CNN) to estimate BP from PPG signals then conducted transfer learning to estimate BP from rPPG signals extracted via POS [69]. They applied a personalization technique, which re-trains the CNN with person-specific data, to improve BP estimation performance. Although previous methods often require physical characteristics of the individual (*e.g.*, age, BMI) [36, 44, 77] or personalization with person-specific data [42, 60, 71], our U-FaceBP does not use them. We are the first to introduce uncertainty into face video-based BP estimation. In addition, while previous methods rely on rPPG signals extracted using signal processing approaches, we also incorporate BP estimation using PPG signals predicted from face videos via deep learning and BP estimation using face images.

Uncertainty in Deep Learning: While deep learning has become a crucial part of various real-world applications, further transparency of NNs is necessary in high-risk fields such as medical image analysis [49] and autonomous vehicle control [18]. To overcome these limitations, researchers have increased their interest in estimating uncertainty in deep learning [22]. A common way to estimate uncertainty in an NN is Bayesian inference [7, 20, 30, 32, 48]. Kendall *et al.* [30] developed a BNN that captures both aleatoric (referred to as data) and epistemic (referred to as model) uncertainties together in a single model. They investigated that aleatoric uncertainty captures noise inherent in the observations and epistemic uncertainty captures model ignorance. Another way to estimate uncertainty is ensemble approaches [34, 67, 70]. Lakshminarayanan *et al.* [34] showed that shuffling the training data and a random initialization of the training process induces a sufficient variety in the models. They estimated uncertainty by evaluating the variety among multiple models. U-FaceBP introduces Bayesian ensemble deep learning, which employs both Bayesian inference and ensemble approaches, enabling us to evaluate uncertainty from various perspectives.

3. Method

The framework of U-FaceBP is illustrated in Fig. 2. We first introduce uncertainty in Bayesian deep learning in Sec. 3.1. We then explain BP estimation from rPPG signals, PPG signals, and face images in Secs. 3.2, 3.3, and 3.4, respectively. Finally, we explain the estimation of BP and uncertainties in Sec. 3.5.

3.1. Uncertainty in Bayesian Deep Learning

U-FaceBP introduces data and model uncertainties [30] using a BNN [15, 45, 50]. To capture model uncertainty in an NN, a BNN sets a prior distribution over its weights, such as

a Gaussian prior distribution: $\mathbf{W} \sim \mathcal{N}(0, I)$. This replaces the deterministic weight parameters in the NN with distributions over those parameters. Denoting the random output of the BNN as $\mathbf{f}^{\mathbf{W}}(\mathbf{x})$ and ground-truth BP as \mathbf{y} , the model likelihood is defined as $p(\mathbf{y}|\mathbf{f}^{\mathbf{W}}(\mathbf{x}))$. Since BP estimation is a regression task, U-FaceBP defines the likelihood as a Gaussian distribution: $p(\mathbf{y}|\mathbf{f}^{\mathbf{W}}(\mathbf{x})) = \mathcal{N}(\mu(\mathbf{x}), \sigma(\mathbf{x})^2)$. Here, $\mu(\mathbf{x})$ is the predictive mean when \mathbf{x} is input into the model. Also, $\sigma(\mathbf{x})^2$ is the observation noise (predictive variance) that represents data uncertainty depending on the input \mathbf{x} , referred to as heteroscedastic uncertainty.

Given a dataset with input \mathbf{X} and output \mathbf{Y} , Bayesian inference is used to compute the posterior over the weights $p(\mathbf{W}|\mathbf{X}, \mathbf{Y}) = p(\mathbf{Y}|\mathbf{X}, \mathbf{W})p(\mathbf{W})/p(\mathbf{Y}|\mathbf{X})$. Since $p(\mathbf{Y}|\mathbf{X})$ cannot be calculated analytically, the posterior $p(\mathbf{W}|\mathbf{X}, \mathbf{Y})$ is approximated with a simple distribution $q_{\theta}^*(\mathbf{W})$. We use variational inference with Monte Carlo (MC) dropout [21] to find $q_{\theta}^*(\mathbf{W})$ that minimizes the Kullback-Leibler (KL) divergence to the true posterior $p(\mathbf{W}|\mathbf{X}, \mathbf{Y})$. MC dropout is conducted by training the model with dropout in each weight layer and by also conducting dropout during testing to sample from the approximate posterior. U-FaceBP, as also an ensemble method, estimates BP from face videos with multiple BNNs. In the following sections, we discuss adapting the BNN described in this section to each ensemble network.

3.2. BP Estimation from rPPG Signals

As a training dataset, we use a set of face videos \mathbf{X} , systolic BP (SBP) \mathbf{Y}_{sbp} , and diastolic BP (DBP) \mathbf{Y}_{dbp} , denoted as $(\mathbf{X}, \mathbf{Y}_{\text{sbp}}, \mathbf{Y}_{\text{dbp}}) = \{\mathbf{X}_i, y_{\text{sbp},i}, y_{\text{dbp},i}\}_{i=1}^N$, where i is the sample index and N is the number of samples. We extract rPPG signals from face videos then estimate BP on the basis of the BNN. We first apply face detection [27] to the face videos and detect face feature points. Then, rPPG signals are extracted from multiple regions of interests (ROIs) on the face. As in a previous study [72], we extract rPPG signal $\mathbf{X}_i^{\text{rPPG}} \in \mathbb{R}^{K \times F}$ from three ROIs on the cheek, inner cheek, and forehead (see Fig. 2 (a)) using POS [69]. Note that K is the number of ROIs and F is the number of frames ($K = 3$ and $F = 150$ in our experiment). By extracting rPPG signals in multiple ROIs, we can use both pulse waveform and PTT features. Specifically, the pulse waveform of rPPG signals contains BP-related features [71], and rPPG signals from multiple ROIs (*e.g.*, cheek and forehead) contain PTT-related features [72].

BP is then estimated from rPPG signals $\mathbf{X}_i^{\text{rPPG}}$ using the BNN. We use S-Net [72], which is used for BP estimation from rPPG signals, as the backbone of the BNN. Therefore, the model outputs the predictive mean and variance, as shown in Sec. 3.1. Specifically, there are four outputs: SBP’s predictive mean $\hat{y}_{\text{sbp},i}^{\text{rPPG}}$ and variance $(\hat{\sigma}_{\text{sbp},i}^{\text{rPPG}})^2$ and DBP’s predictive mean $\hat{y}_{\text{dbp},i}^{\text{rPPG}}$ and variance $(\hat{\sigma}_{\text{dbp},i}^{\text{rPPG}})^2$. MC

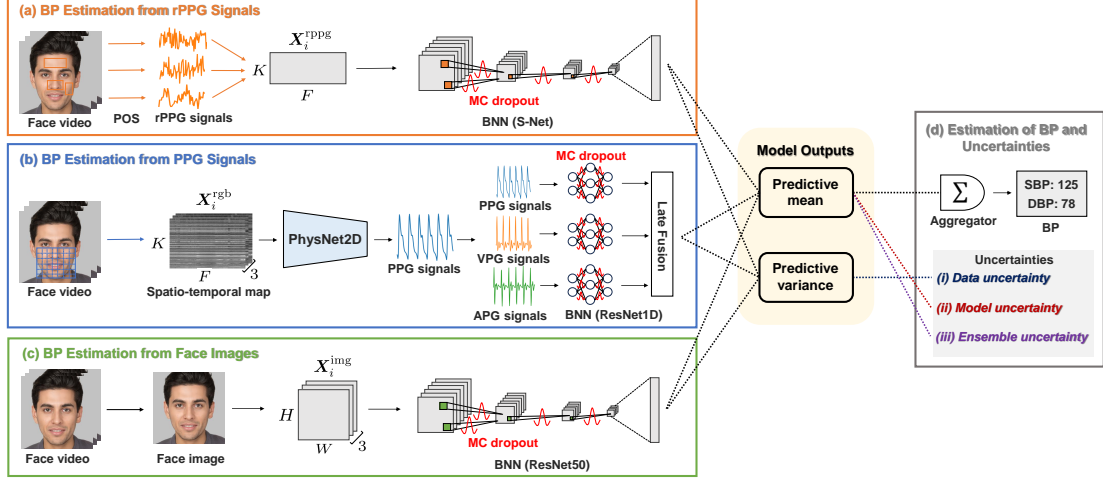


Figure 2. Framework of U-FaceBP: (a) BP estimation from rPPG signals (Sec. 3.2), (b) BP estimation from PPG signals (Sec. 3.3), (c) BP estimation from face images (Sec. 3.4), and (d) estimation of BP and uncertainties (Sec. 3.5). Face photo by Generated Photos [2].

dropout is then carried out by implementing dropout after each residual block in S-Net during training and testing to sample the approximate posterior $\widehat{\mathbf{W}} \sim q_{\theta}^*(\mathbf{W})$. The BNN is optimized on the basis of the following loss function [30]:

$$\mathcal{L}_{\text{rPPG}}(\theta) = \frac{1}{N} \sum_{i=1}^N \frac{\|y_{\text{sbp},i} - \hat{y}_{\text{sbp},i}^{\text{rPPG}}\|^2}{2(\hat{\sigma}_{\text{sbp},i}^{\text{rPPG}})^2} + \frac{1}{2} \log(\hat{\sigma}_{\text{sbp},i}^{\text{rPPG}})^2 + \frac{1}{N} \sum_{i=1}^N \frac{\|y_{\text{dbp},i} - \hat{y}_{\text{dbp},i}^{\text{rPPG}}\|^2}{2(\hat{\sigma}_{\text{dbp},i}^{\text{rPPG}})^2} + \frac{1}{2} \log(\hat{\sigma}_{\text{dbp},i}^{\text{rPPG}})^2. \quad (1)$$

In the first terms for SBP (first row) and DBP (second row), the predictive variances $(\hat{\sigma}_{\text{sbp},i}^{\text{rPPG}})^2$ and $(\hat{\sigma}_{\text{dbp},i}^{\text{rPPG}})^2$ enable the model to be trained while handling data uncertainty. More specifically, large predictive variances work to ignore regression loss, while small predictive variances work to emphasize regression loss. In BP estimation, there are data uncertainties such as uncertainty of BP estimation from pulse waves and individual differences in the cardiovascular system, and terms of predictive variance handle these uncertainties. Although it is difficult to define the labels for data uncertainty, we can implicitly learn data uncertainty (*i.e.*, predictive variance) by optimizing the network on the basis of the loss function. The second terms $\frac{1}{2} \log(\hat{\sigma}_{\text{sbp},i}^{\text{rPPG}})^2$ and $\frac{1}{2} \log(\hat{\sigma}_{\text{dbp},i}^{\text{rPPG}})^2$ prevent the network from predicting infinite uncertainty (*i.e.*, zero loss) for all samples. In practice, we train the network to predict the log variances $s_{\text{sbp},i}^{\text{rPPG}} := \log(\hat{\sigma}_{\text{sbp},i}^{\text{rPPG}})^2$ and $s_{\text{dbp},i}^{\text{rPPG}} := \log(\hat{\sigma}_{\text{dbp},i}^{\text{rPPG}})^2$ for numerical stability as in a previous study [30]. Therefore, we train a BP estimation network from rPPG signals on the basis of $\mathcal{L}_{\text{rPPG}}(\theta)$.

3.3. BP Estimation from PPG Signals

The rPPG signals mentioned in Sec. 3.2 are hand-crafted features extracted using a signal processing approach [69],

so the quality of pulse waves may be low. Deep learning-based PPG signal estimation from face video has achieved robustness to noise due to body motion and lighting environment [3, 11, 40, 76]. To precisely and robustly extract the pulse waveform, we estimate the PPG signal $\mathbf{p}_i \in \mathbb{R}^{D_p}$ from the face video using deep learning then estimate BP from the estimated PPG signal. Note that D_p is the dimension of the PPG signal acquired from the contact-type PPG sensor. Importantly, rPPG signals contain PTT-related features unlike PPG signals, so both rPPG and PPG signals provide different information related to BP.

We first extract RGB signals from face videos then estimate PPG signals on the basis of deep learning, in a similar manner to a previous study [3]. We define 16×14 blocks for the area under the eyes (see Fig. 2 (b)) and create multiple ROIs by arranging them. We then construct a spatio-temporal map $\mathbf{X}_i^{\text{rgb}} \in \mathbb{R}^{3 \times K \times F}$ using RGB time-series signals (3 being RGB channels, $K = 224$, and $F = 150$ in our experiment). We use PhysNet2D [3] as a deep learning model, which outputs the PPG signal $\hat{\mathbf{p}}_i \in \mathbb{R}^{D_p}$ from the spatio-temporal map $\mathbf{X}_i^{\text{rgb}}$. As the loss function between $\hat{\mathbf{p}}_i$ and \mathbf{p}_i , we use the mean squared error (MSE) loss to minimize the error in the pulse waveform (different from the above previous study [3]). Furthermore, inspired by previous studies [38, 61], we use the first derivative (VPG signal) $\mathbf{p}'_i \in \mathbb{R}^{D_p-1}$ and second derivative (APG signal) $\mathbf{p}''_i \in \mathbb{R}^{D_p-2}$ of the PPG signal. These derivatives contain the information about aortic compliance and stiffness, which is highly related to BP [38]. Thus, we train PhysNet2D with the following loss function: $\mathcal{L}_{\text{pulse}} = \frac{\alpha}{N} \sum_{i=1}^N \|\mathbf{p}_i - \hat{\mathbf{p}}_i\|^2 + \frac{\beta}{N} \sum_{i=1}^N \|\mathbf{p}'_i - \hat{\mathbf{p}}'_i\|^2 + \frac{\gamma}{N} \sum_{i=1}^N \|\mathbf{p}''_i - \hat{\mathbf{p}}''_i\|^2$, where α , β , and γ are hyperparameters that control the weight of each loss. Note that $\hat{\mathbf{p}}'_i$ and $\hat{\mathbf{p}}''_i$ are obtained from the first and second derivatives of the estimated PPG signal $\hat{\mathbf{p}}_i$, respectively.

BP is then estimated from the PPG \hat{p}_i , VPG \hat{p}'_i , and APG signals \hat{p}''_i using the BNN. We use ResNet1D [60], which is used for BP estimation from PPG signals, as the backbone of the BNN. U-FaceBP concatenates the feature representations obtained from each ResNet1D corresponding to PPG, VPG, and APG signals then outputs the predictive mean and variance (see Fig. 2 (b)). The BNN is optimized on the basis of the loss function $\mathcal{L}_{\text{ppg}}(\theta)$ in the same manner as in Eq. (1). Overall, U-FaceBP trains the network in an end-to-end fashion using the loss function $\mathcal{L}_{\text{pulse}} + \mathcal{L}_{\text{ppg}}(\theta)$.

3.4. BP Estimation from Face Images

The face images contain BP-related information, such as age, BMI [72, 73], facial shape [4, 62], wrinkles, and baldness [37, 41]. The pulse waves and face images have complementary BP-related information, so the ensemble approach improves the BP estimation performance.

We obtain a face image $\mathbf{X}_i^{\text{img}} \in \mathbb{R}^{3 \times H \times W}$ (H and W being the height and width of the image, respectively). Note that the images include the entire face to capture baldness. We estimate BP from face images $\mathbf{X}_i^{\text{img}}$ using the BNN with ResNet50 [26] as the backbone. Since the number of face images paired with BPs for training data is limited, pre-training the BNN is essential. We leverage a pre-trained model on the basis of facial representation learning (FRL) [8], which is useful for various face tasks. Specifically, FRL [8] performs SwAV [9]-based self-supervised learning using unlabeled face images to acquire feature representations related to human faces. We then carry out fine-tuning (*i.e.*, transfer learning of all layers) of the BNN using the loss function $\mathcal{L}_{\text{img}}(\theta)$ in the same manner as in Eq. (1).

3.5. Estimation of BP and Uncertainties

We predict the BP and calculate the uncertainty using the ensemble method with multiple BNNs. We explain this only for SBP, but the same applies to DBP.

We first explain the prediction of SBP. At test time, we sample T times according to MC dropout, and use the mean of these predictions. Specifically, the predicted SBP from the rPPG signal is calculated as $\hat{y}_{\text{sbp}}^{\text{rppg}} = \frac{1}{T} \sum_{t=1}^T \hat{y}_{\text{sbp},t}^{\text{rppg}}$, where $\hat{y}_{\text{sbp},t}^{\text{rppg}}$ indicates the predictive mean of the SBP estimated from the rPPG signal at the t -th sampling. This is the same for calculating SBPs $\hat{y}_{\text{sbp}}^{\text{ppg}}$ and $\hat{y}_{\text{sbp}}^{\text{img}}$ predicted from the PPG signal and face image, respectively. The predicted SBP is then aggregated using the ensemble method as $\hat{y}_{\text{sbp}} = (\hat{y}_{\text{sbp}}^{\text{rppg}} + \hat{y}_{\text{sbp}}^{\text{ppg}} + \hat{y}_{\text{sbp}}^{\text{img}})/3$.

An important function of U-FaceBP is the calculation of uncertainty. By understanding the prediction confidence through uncertainty, we can flexibly handle the predicted BP. We can also improve the transparency of deep learning models for face video-based BP estimation. We first calculate data and model uncertainties [30]. The data uncertainty for estimating the SBP from the rPPG signal is calculated as

$U_{\text{rppg, sbp}}^{\text{data}} = \frac{1}{T} \sum_{t=1}^T (\hat{\sigma}_{\text{sbp},t}^{\text{rppg}})^2$, where $(\hat{\sigma}_{\text{sbp},t}^{\text{rppg}})^2$ represents the predictive variance of the SBP estimated from the rPPG signal at the t -th sampling. The data uncertainty is defined by the predictive variance used in Eq. (1). The model uncertainty for estimating the SBP from the rPPG signal is calculated as $U_{\text{rppg, sbp}}^{\text{model}} = \frac{1}{T} \sum_{t=1}^T (\hat{y}_{\text{sbp},t}^{\text{rppg}})^2 - (\frac{1}{T} \sum_{t=1}^T \hat{y}_{\text{sbp},t}^{\text{rppg}})^2$. The model uncertainty is defined as the variance of the predictive mean over T samples. These are the same for calculating the data and model uncertainties $U_{\text{ppg, sbp}}^{\text{data}}$, $U_{\text{ppg, sbp}}^{\text{model}}$ and $U_{\text{img, sbp}}^{\text{data}}$, $U_{\text{img, sbp}}^{\text{model}}$ estimated from the PPG signal and face image, respectively.

We then calculate ensemble uncertainty using the predictions from multiple BNNs. The ensemble uncertainty is calculated as $U_{\text{sbp}}^{\text{ens}} = \frac{1}{3} \{(\hat{y}_{\text{sbp}}^{\text{rppg}})^2 + (\hat{y}_{\text{sbp}}^{\text{ppg}})^2 + (\hat{y}_{\text{sbp}}^{\text{img}})^2\} - (\frac{1}{3} \{\hat{y}_{\text{sbp}}^{\text{rppg}} + \hat{y}_{\text{sbp}}^{\text{ppg}} + \hat{y}_{\text{sbp}}^{\text{img}}\})^2$, which is defined as the variance in the predictive mean from the rPPG, PPG signals, and face image. Finally, the uncertainty for SBP is calculated as the sum of the uncertainties $U_{\text{sbp}} = U_{\text{rppg, sbp}}^{\text{data}} + U_{\text{ppg, sbp}}^{\text{data}} + U_{\text{img, sbp}}^{\text{data}} + U_{\text{rppg, sbp}}^{\text{model}} + U_{\text{ppg, sbp}}^{\text{model}} + U_{\text{img, sbp}}^{\text{model}} + U_{\text{sbp}}^{\text{ens}}$. We can consider the predicted SBP to be highly reliable if the uncertainty U_{sbp} is small, or vice versa.

4. Experiments

We use a large-scale dataset, focusing on the pitfalls [47] of the experimental setting in BP estimation. Mehta *et al.* [47] demonstrated that previous studies often misleadingly provide lower estimation errors than actual values. Specifically, data leakage such as including the same subjects in both the training and test data, and task constraints such as limiting to subjects with normal BP ranges, have made the prediction task artificially “easier”. Therefore, we design our experiment on the basis of these points.

4.1. Dataset

Since there are no publicly available datasets (approved by institutional review board) for face video-based BP measurement, we collected a large amount of data including face videos, BPs, and PPG signals. Note that our data collection was approved by an ethical review board. The number of subjects is 786 (mainly East Asians, ages: 20s to 90s, genders: 432 males and 354 females, see the supplement for details), which is comparable to the large-scale datasets of previous studies [36, 72]. We captured face videos using a webcam for 1 minute while the subject was seated, and simultaneously acquired BP from an electronic sphygmomanometer (A&D UA-1200BLE) and PPG signals from a PPG sensor attached to the fingertip (Plux blood volume pulse sensor). A Logitech C920n webcam was used at 30 frames per second. If 1 minute of recording was considered one set, each subject participated in between two and five sets. Some of the subjects participated in recordings over several days. Our dataset consists of a total of 2211 sets, and includes subjects with a wide range of BPs (see Fig. 3).

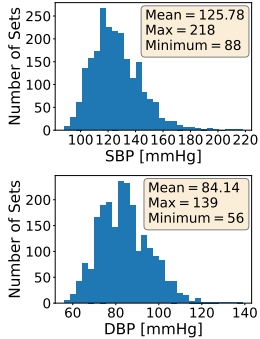


Figure 3. BP distribution in our dataset.

Table 1. Performance comparison with benchmark and state-of-the-art (SoTA) BP estimation methods in 5-fold cross-validation using our dataset. Estimation performance improves when evaluation metric given \downarrow is lower and evaluation metric given \uparrow is higher. Best results are marked in **bold**.

Method	SBP					DBP				
	MAE \downarrow	STD \downarrow	Corr. \uparrow	Suc5 \uparrow	Suc10 \uparrow	MAE \downarrow	STD \downarrow	Corr. \uparrow	Suc5 \uparrow	Suc10 \uparrow
Mean Regressor	13.87	17.74	-0.086	21.9	43.7	9.48	11.97	-0.055	33.4	58.7
Zhou <i>et al.</i> [77]	13.26	17.21	0.247	25.4	46.6	9.33	11.76	0.208	32.7	60.8
ResNet1D [60]	12.74	15.55	0.477	24.5	45.7	8.69	10.79	0.433	34.2	62.9
AlexNet1D [60]	12.06	15.46	0.493	25.5	50.5	8.56	10.82	0.425	36.0	65.5
S-Net [72]	11.77	15.20	0.512	27.1	51.4	8.48	10.76	0.440	36.8	66.4
FS-Net [72]	11.68	14.95	0.534	27.8	52.1	8.34	10.58	0.468	37.5	67.2
Trirongjitmoah <i>et al.</i> [66]	13.43	17.16	0.241	22.9	45.1	9.13	11.56	0.258	34.8	61.0
Liu <i>et al.</i> [39]	11.84	15.48	0.484	26.7	53.5	8.57	10.87	0.421	35.8	65.0
U-FaceBP (Ours)	10.89	14.05	0.622	28.2	54.8	7.77	9.84	0.580	39.3	70.4

4.2. Experimental Setup

We conduct 5-fold cross-validation in which the data of 80% of the subjects are used as training data and 20% as test data. This verification means that the subjects do not overlap between the training and test data. We use 20% of the training data as validation data for monitoring loss values and tuning hyperparameters. In each epoch, samples of 5 seconds (number of frames $F = 150$) are randomly sampled and used for training the model. We sample in the same manner during testing, and use the average of these estimated results. The hyperparameters of the loss function $\mathcal{L}_{\text{pulse}}$ are set to $\alpha = 5$, $\beta = 10$, and $\gamma = 15$. The sampling number for MC dropout is set to $T = 10$. For BP estimation from rPPG and PPG signals, to prevent the estimated BPs from being concentrated around the mean BP, the training data are doubly upsampled when the SBP is below 110 or above 150 mmHg, or the DBP is below 70 or above 100 mmHg. For BP estimation from face images, the images are resized to $H = 224$ and $W = 224$, and random crop, horizontal flip, color jitter, and grayscale are used as data augmentation. The BP values are normalized to mean 0 and standard deviation 1. For all models, we train for 30 epochs and use the model at the epoch with the lowest validation loss for testing. The optimization algorithm is Adam [31], batch size is 128, and learning rates are $1e-3$, $1e-3$, and $1e-4$ for BP estimation from rPPG, PPG signals, and face images, respectively. Our models are implemented with PyTorch [56] and trained on eight A100 GPUs.

4.3. Main Results

Performance Comparison with SoTA: We first compare our U-FaceBP with the eight benchmark and SoTA BP estimation methods listed in Table 1 using our dataset. Mean Regressor is a benchmark method that always predicts the mean SBP and DBP of the training data. ResNet1D [60], AlexNet1D [60], S-Net [72], and Trirongjitmoah *et al.* [66] estimate BP from rPPG signals. Zhou *et al.* [77] and FS-Net [72] estimate BP from rPPG signals and additional information such as BMI estimated from face images. Liu

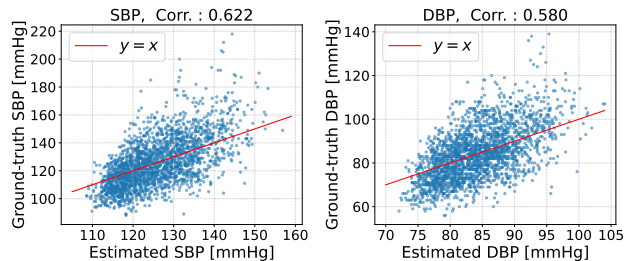


Figure 4. Correlation plots of SBP and DBP in our U-FaceBP.

et al. [39] is an end-to-end BP estimation method from RGB frames of face videos, which won first place in the face video-based BP estimation task in the 3rd RePSS challenge [63]. See the supplement for details on the implementation of the comparison methods. We use mean absolute error (MAE), standard deviation of error (STD), Pearson correlation coefficient (Corr.), and the percentage of predictions with absolute error below 5 or 10 mmHg (Suc5 or Suc10), which were commonly used in previous studies [36, 72], as the evaluation metrics.

Table 1 shows the performance comparison with the benchmark and SoTA BP estimation methods. The MAEs for SBP and DBP in Mean Regressor are 13.87 and 9.48, respectively, and no correlation is observed (*i.e.*, Corr. is almost zero). Some methods are slightly better than Mean Regressor, which is similar to the results reported in previous studies [60, 72]. The best performance of the comparison methods is achieved with FS-Net [72], with MAEs of 11.68 and 8.34 for SBP and DBP, respectively. Our U-FaceBP achieves the best performance in all evaluation metrics compared to other methods, with MAEs of 10.89 and 7.77 for SBP and DBP, respectively. We conduct Wilcoxon signed-rank tests for absolute errors in all predictions between U-FaceBP and all other methods and confirm statistically significant differences ($p < 0.01$). Note that we use a Bonferroni correction for multiple tests. Figure 4 shows the correlation plots of SBP and DBP with U-FaceBP. The correlation coefficients of SBP and DBP are 0.622 and 0.580, respectively, indicating a moderately strong positive corre-

Table 2. Inter-dataset performance comparison. Performance improves when mean absolute scale error (MASE) is lower.

Study	Input	SBP	DBP
		MASE↓	MASE↓
Schrumpf <i>et al.</i> [60]	Face video	97.2	93.0
Wu <i>et al.</i> [72]	Face video	86.8	93.4
Wu <i>et al.</i> [71]	Face video	81.2	89.2
González <i>et al.</i> [25]	PPG signals*	79.8	90.2
Ours	Face video	78.5	82.0

*acquired from PPG sensor

lation between the estimated and ground-truth BPs.

Inter-dataset Performance Comparison: We then compare our BP estimation performance with those reported in the four previous studies listed in Table 2. Schrumpf *et al.* [60], Wu *et al.* [72], and Wu *et al.* [71] evaluated the performance of BP estimation from face videos using the datasets created for each study. González *et al.* [25] conducted a benchmark study of BP estimation from PPG signals and conducted an extensive performance comparison using 4 different datasets and 11 different machine learning methods. Since the range of BPs differs depending on the dataset, it is difficult to compare performance fairly between datasets (estimation errors tend to be larger when the range of BPs is wider). Therefore, we use mean absolute scale error (MASE) proposed by González *et al.* [25] to compare performance between datasets. MASE is the ratio of MAE of the model to that of Mean Regressor and calculates the estimation error after standardizing the difficulty of the estimation task. When multiple methods were proposed in each of the previous studies, the MASE of the method with the best performance for SBP and DBP is reported.

Table 2 shows the inter-dataset performance comparison. Our study outperforms previous face video-based BP estimation studies by Schrumpf *et al.* [60], Wu *et al.* [72], and Wu *et al.* [71]. Remarkably, our U-FaceBP performs better than González *et al.* [25], who conducted a comprehensive performance evaluation of BP estimation from PPG signals. This suggests that we can estimate BP from face videos with a lower estimation error than not only the error reported from previous BP estimation using face videos, but also from BP estimation using contact-based PPG sensors.

4.4. Ablation Study

We ablate the components of U-FaceBP to verify the effectiveness of the following factors.

Ensemble Components of U-FaceBP: Table 3 shows the performance comparison among the ensemble components of U-FaceBP. The BP estimation models using only rPPG, PPG signals, or face images have comparable performance (all of these are overall better than previous methods in Table 1). BP estimation from PPG signals is slightly better, demonstrating the benefits of estimating precise

Table 3. Performance comparison among components of ensemble method. Bottom row denotes late fusion model of rPPG, PPG signals, and face images. Shading indicates our final setting.

Ensemble	SBP		DBP	
	MAE↓	Corr.↑	MAE↓	Corr.↑
rPPG	11.60	0.541	8.21	0.494
PPG**	11.46	0.560	8.22	0.509
Face images	11.51	0.516	8.28	0.481
rPPG+PPG**	11.20	0.595	8.00	0.539
rPPG+Face images	10.95	0.604	7.80	0.569
PPG**+Face images	11.01	0.594	7.87	0.556
rPPG+PPG**+Face images	10.89	0.622	7.77	0.580
Late Fusion	12.05	0.479	8.73	0.436

**estimated from face videos

Table 4. Ablation study for Bayesian neural network (BNN), derivatives of PPG signal (Deri), and facial representation learning (FRL). Shading indicates our final setting.

	BNN	Deri	FRL	SBP		DBP	
				MAE↓	Corr.↑	MAE↓	Corr.↑
(a)		✓	✓	11.13	0.602	7.85	0.574
(b)	✓		✓	10.96	0.618	7.80	0.576
(c)	✓	✓		10.93	0.618	7.80	0.570
(d)	✓	✓	✓	10.89	0.622	7.77	0.580

pulse waveforms from face videos. The performance of “rPPG+PPG” is better than that of each individual component, and the incorporation of face images further improves the performance of rPPG or PPG signals. These results suggest that each of the three components provides complementary information related to BP. Ultimately, “rPPG+PPG+Face images” exhibits the best performance.

Ensemble vs. Late Fusion: Although we use an ensemble approach using rPPG, PPG signals, and face images, the feature fusion of these components is a straightforward approach. The bottom row in Table 3 indicates the BP estimation performance of the single BNN model that concatenates the feature representations of the three components using late fusion (the number of trainable parameters for ensemble and late fusion are comparable). Unexpectedly, the late fusion model significantly degrades performance compared with the ensemble approach. This may be because if one modality makes an inaccurate prediction, it negatively affects the late fusion model [64]. On the other hand, ensemble methods are not easily affected by a single modality, resulting in a superior performance to late fusion [12].

Uncertainty-aware Network: Table 4 (a,d) compares the performance of a standard NN and BNN (the number of trainable parameters for NN and BNN are comparable). We can see that introducing BNNs into the three ensemble components improves performance. This result indicates the effectiveness of BNNs, which can learn from small or noisy datasets without overfitting by considering uncertainty [28].

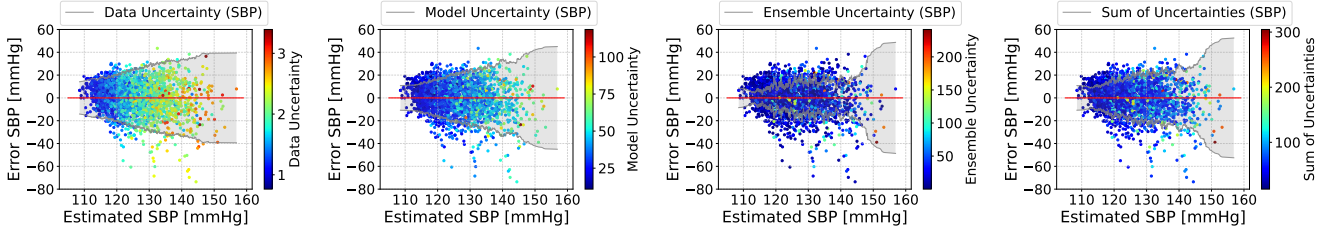


Figure 5. Scatter plots of estimated SBP with U-FaceBP and error of SBP. Four uncertainties are plotted in color, and range of gray lines indicates uncertainty values. Gray lines are smoothed using Savitzky-Golay filter against actual values, and scale is adjusted to figure.

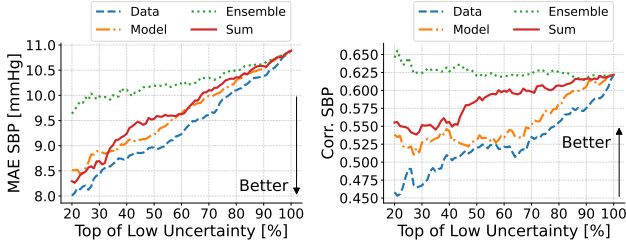


Figure 6. Relationship between top of low uncertainty (top $x\%$ of predictions when predictions are ranked in ascending order of uncertainties) and their MAE and correlation coefficient for SBP.

Derivatives of PPG Signal: Table 4 (b,d) shows the effectiveness of introducing derivatives of PPG signals (*i.e.*, VPG and APG signals in Fig. 2 (b)). The derivatives provide valuable information related to BP (aortic compliance and stiffness [38]), leading to better performance.

Facial Representation Learning: Table 4 (c,d) compares the performance of ImageNet pre-training [14] and facial representation learning (FRL) [8] for BP estimation from face images. Leveraging FRL achieves better BP estimation performance than commonly used ImageNet pre-training.

4.5. Uncertainties

Finally, we thoroughly investigate uncertainties. Figure 5 shows the relationship between estimated SBP with U-FaceBP and the error of SBP (see the supplement for DBP results). Simultaneously, the data, model, ensemble, and sum of uncertainties are illustrated, where the uncertainty is higher when the gray line is wider. The data uncertainty tends to be larger when the estimated SBP is higher, reflecting the fact that the error can be large for SBP above 120 mmHg in some cases (*e.g.*, errors from -40 to -80 mmHg). This suggests that BP estimation is difficult when SBP is high, *i.e.*, the predictive variance in Eq. (1) is difficult to reduce. This difficulty is associated with the fact that hypertension has a wide BP range (from 140 to 218 mmHg for SBP in our dataset). The model uncertainty gradually increases for SBP above 140 mmHg, where the training data are insufficient (see Fig. 3), and exactly reflects the lack of knowledge of the model. The ensemble uncertainty is similar over a relatively wide range of SBP values, indicating

that the confidence in the predictions from multiple models is widely maintained. Since there are few prediction cases above 145 mmHg among multiple models, the ensemble uncertainty increases rapidly. The sum of uncertainties aggregates the trends of the three uncertainties, showing a tendency to be larger when the predicted SBP is high.

Figure 6 shows the relationship between uncertainties and estimation performance. The horizontal axis of Fig. 6 represents the top $x\%$ of predictions when the predictions are ranked in ascending order of uncertainties, referred to as “top of low uncertainty”. The MAE is smaller when the four uncertainties are lower, indicating that lower uncertainty leads to better performance. In particular, the data, model, and sum of uncertainties perform equally well. On the other hand, the correlation coefficient improves when the ensemble uncertainty is low. The low data and model uncertainties tend to concentrate on low SBP predictions, leading to poor correlation coefficients. The sum of uncertainties has the best balance of MAE and correlation coefficient and successfully captures the relationship between uncertainty and estimation performance. Therefore, we can handle prediction confidence using the sum of uncertainties and increase the transparency of deep learning models. See the supplement for other analyses of uncertainties.

5. Conclusions and Future Work

We propose an uncertainty-aware Bayesian ensemble deep learning method for face video-based BP measurement called U-FaceBP. With the introduction of uncertainty and a powerful ensemble approach, our U-FaceBP outperforms the SoTA methods. We also show that the prediction confidence and estimation performance are correlated. Research on face video-based BP measurement is still in its early stages, and this study has the following limitations: (i) subjects are limited to East Asians, (ii) the estimation error is large for severe hypertension (SBP above 160 mmHg and DBP above 105 mmHg), and (iii) our results do not meet the medical requirements for BP measurement devices (*e.g.*, Grade C of the British Hypertension Society standard [53] requires $\text{Suc}_5 \geq 40\%$ and $\text{Suc}_{10} \geq 65\%$ in Table 1). Future work should collect data from subjects with diverse skin tones, include sufficient training data on severe hypertension, and aim to meet the medical standards.

References

- [1] Illinois doc labeled faces dataset. <https://www.kaggle.com/davidjfisher/illinois-doc-labeled-faces-dataset>. 1
- [2] Generated Photos. <https://generated.photos/>. 4
- [3] Y. Akamatsu, T. Umematsu, and H. Imaoka. CalibrationPhys: Self-supervised video-based heart and respiratory rate measurements by calibrating between multiple cameras. *IEEE Journal of Biomedical and Health Informatics*, 28: 1460–1471, 2024. 4
- [4] L. Ang, M. H. Yim, J. Do, and S. Lee. A novel method in predicting hypertension using facial images. *Applied Sciences*, 11(5):2414, 2021. 2, 5
- [5] J. Bae and Y. J. Jeon. Pulse sharpness as a quantitative index of vascular aging. *Scientific Reports*, 11(1):19895, 2021. 4
- [6] R. C. Block, M. Yavarimanesh, K. Natarajan, A. Carek, et al. Conventional pulse transit times as markers of blood pressure changes in humans. *Scientific Reports*, 10(1):16373, 2020. 1
- [7] C. Blundell, J. Cornebise, K. Kavukcuoglu, and D. Wierstra. Weight uncertainty in neural network. In *Proc. Int. Conf. Machine Learning (ICML)*, pages 1613–1622, 2015. 3
- [8] A. Bulat, S. Cheng, J. Yang, A. Garbett, et al. Pre-training strategies and datasets for facial representation learning. In *Proc. European Conf. Computer Vision (ECCV)*, pages 107–125, 2022. 5, 8
- [9] M. Caron, I. Misra, J. Mairal, P. Goyal, et al. Unsupervised learning of visual features by contrasting cluster assignments. In *Proc. Advances in Neural Information Processing Systems (NeurIPS)*, pages 9912–9924, 2020. 5
- [10] KW Chan, K Hung, and YT Zhang. Noninvasive and cuffless measurements of blood pressure for telemedicine. In *Proc. Annual Int. Conf. IEEE Engineering in Medicine and Biology Society (EMBC)*, pages 3592–3593, 2001. 1
- [11] W. Chen and D. McDuff. DeepPhys: Video-based physiological measurement using convolutional attention networks. In *Proc. European Conference on Computer Vision (ECCV)*, pages 349–365, 2018. 4
- [12] K. Choudhury, R. Murugan, M. Azharuddin Laskar, and Rabul H. Laskar. A comparative analysis between late fusion of features approach and ensemble of multiple classifiers approach for image classification. *Concurrency and Computation: Practice and Experience*, 33(20):e6371, 2021. 7
- [13] G. De Haan and V. Jeanne. Robust pulse rate from chrominance-based rPPG. *IEEE Transactions on Biomedical Engineering*, 60(10):2878–2886, 2013. 2
- [14] J. Deng, W. Dong, R. Socher, L. Li, et al. ImageNet: A large-scale hierarchical image database. In *Proc. IEEE/CVF Conf. Computer Vision and Pattern Recognition (CVPR)*, pages 248–255, 2009. 8, 1
- [15] J. Denker and Y. LeCun. Transforming neural-net output levels to probability distributions. *Proc. Advances in Neural Information Processing Systems (NeurIPS)*, 3, 1990. 3
- [16] A. Diaz, M. Tringler, Sandra Wray, Agustín J R., et al. The effects of age on pulse wave velocity in untreated hypertension. *The Journal of Clinical Hypertension*, 20(2):258–265, 2018. 4
- [17] WB. Drøyvold, K. Midthjell, TIL. Nilsen, and J. Holmen. Change in body mass index and its impact on blood pressure: a prospective population study. *International Journal of Obesity*, 29(6):650–655, 2005. 2
- [18] D. Feng, L. Rosenbaum, and K. Dietmayer. Towards safe autonomous driving: Capture uncertainty in the deep neural network for lidar 3D vehicle detection. In *Proc. Int. Conf. Intelligent Transportation Systems (ITSC)*, pages 3266–3273, 2018. 3
- [19] L. Frey, C. Menon, and M. Elgendi. Blood pressure measurement using only a smartphone. *NPJ Digital Medicine*, 5(1):86, 2022. 1, 2
- [20] Y. Gal and Z. Ghahramani. Bayesian convolutional neural networks with Bernoulli approximate variational inference. *arXiv preprint arXiv:1506.02158*, 2015. 3
- [21] Y. Gal and Z. Ghahramani. Dropout as a Bayesian approximation: Representing model uncertainty in deep learning. In *Proc. Int. Conf. Machine Learning (ICML)*, pages 1050–1059, 2016. 3
- [22] J. Gawlikowski, C. R. N. Tassi, M. Ali, J. Lee, et al. A survey of uncertainty in deep neural networks. *Artificial Intelligence Review*, 56(Suppl 1):1513–1589, 2023. 3
- [23] LA Geddes, MH Voelz, CF Babbs, JD Bourland, et al. Pulse transit time as an indicator of arterial blood pressure. *Psychophysiology*, 18(1):71–74, 1981. 1
- [24] H. Gesche, D. Grosskurth, G. Küchler, and A. Patzak. Continuous blood pressure measurement by using the pulse transit time: comparison to a cuff-based method. *European Journal of Applied Physiology*, 112(1):309–315, 2012. 1
- [25] S. González, W. Hsieh, and T. P. Chen. A benchmark for machine-learning based non-invasive blood pressure estimation using photoplethysmogram. *Scientific Data*, 10(1):149, 2023. 7, 1, 2
- [26] K. He, X. Zhang, S. Ren, and J. Sun. Deep residual learning for image recognition. In *Proc. IEEE/CVF Conf. Computer Vision and Pattern Recognition (CVPR)*, pages 770–778, 2016. 5, 1
- [27] H. Imaoka, H. Hashimoto, K. Takahashi, A. F. Ebihara, et al. The future of biometrics technology: from face recognition to related applications. *APSIPA Transactions on Signal and Information Processing*, 10, 2021. 3
- [28] L. V. Jospin, H. Laga, F. Boussaid, W. Buntine, and M. Benamoun. Hands-on Bayesian neural networks—a tutorial for deep learning users. *IEEE Computational Intelligence Magazine*, 17(2):29–48, 2022. 7
- [29] M. Kachuee, M. M. Kiani, H. Mohammadzade, and M. Shabany. Cuffless blood pressure estimation algorithms for continuous health-care monitoring. *IEEE Transactions on Biomedical Engineering*, 64(4):859–869, 2016. 1
- [30] A. Kendall and Y. Gal. What uncertainties do we need in Bayesian deep learning for computer vision? *Proc. Advances in Neural Information Processing Systems (NeurIPS)*, 30, 2017. 2, 3, 4, 5
- [31] D. P. Kingma and J. Ba. Adam: A method for stochastic optimization. *arXiv preprint arXiv:1412.6980*, 2014. 6

- [32] D. Krueger, C. Huang, R. Islam, R. Turner, et al. Bayesian hypernetworks. *arXiv preprint arXiv:1710.04759*, 2017. 3
- [33] Y. Kurylyak, F. Lamonaca, and D. Grimaldi. A neural network-based method for continuous blood pressure estimation from a PPG signal. In *Proc. Int. Instrumentation and Measurement Technology Conference (I2MTC)*, pages 280–283, 2013. 1
- [34] B. Lakshminarayanan, A. Pritzel, and C. Blundell. Simple and scalable predictive uncertainty estimation using deep ensembles. *Proc. Advances in Neural Information Processing Systems (NeurIPS)*, 30, 2017. 3
- [35] J. Leitner, P. Chiang, and S. Dey. Personalized blood pressure estimation using photoplethysmography: A transfer learning approach. *IEEE Journal of Biomedical and Health Informatics*, 26(1):218–228, 2021. 1
- [36] Y. Li, M. Wei, Q. Chen, X. Zhu, et al. Hybrid DIDCnet using forehead iPPG for continuous and noncontact blood pressure measurement. *IEEE Sensors Journal*, 23(3):2727–2736, 2022. 2, 3, 5, 6
- [37] S. Lin, Z. Li, B. Fu, S. Chen, et al. Feasibility of using deep learning to detect coronary artery disease based on facial photo. *European Heart Journal*, 41(46):4400–4411, 2020. 2, 5
- [38] M. Liu, L. Po, and H. Fu. Cuffless blood pressure estimation based on photoplethysmography signal and its second derivative. *International Journal of Computer Theory and Engineering*, 9(3):202, 2017. 4, 8
- [39] W. Liu, B. Wu, M. Zhou, X. Zheng, et al. Ensemble deep learning for blood pressure estimation using facial videos. In *Proc. The 3rd Vision-based Remote Physiological Signal Sensing (RePSS) Challenge & Workshop*, pages 1–10, 2024. 6, 1, 2
- [40] X. Liu, J. Fromm, S. Patel, and D. McDuff. Multi-task temporal shift attention networks for on-device contactless vitals measurement. *Proc. Advances in Neural Information Processing Systems (NeurIPS)*, 33:19400–19411, 2020. 4
- [41] X. Liu, X. Yang, R. Song, J. Zhang, et al. VideoCAD: an uncertainty-driven neural network for coronary artery disease screening from facial videos. *IEEE Transactions on Instrumentation and Measurement*, 72:1–12, 2022. 2, 5
- [42] X. Liu, Z. Sun, X. Li, R. Song, et al. VidBP: Detecting blood pressure from facial videos with personalized calibration. In *Proc. Annual Int. Conf. IEEE Engineering in Medicine and Biology Society (EMBC)*, pages 1–5, 2023. 2, 3
- [43] ÁR Lugo-Mata, AS Urich-Landeta, AL Andrades-Pérez, MJ León-Dugarte, et al. Factors associated with the level of knowledge about hypertension in primary care patients. *Medicina Universitaria*, 19(77):184–188, 2017. 1
- [44] H. Luo, D. Yang, A. Barszczyk, N. Vempala, et al. Smartphone-based blood pressure measurement using transdermal optical imaging technology. *Circulation: Cardiovascular Imaging*, 12(8):e008857, 2019. 2, 3
- [45] D. JC. MacKay. A practical Bayesian framework for back-propagation networks. *Neural Computation*, 4(3):448–472, 1992. 3
- [46] P. Man, K. Cheung, N. Sangsiri, W. J. Shek, et al. Blood pressure measurement: From cuff-based to contactless monitoring. *Healthcare*, 10(10):2113, 2022. 1, 2
- [47] S. Mehta, N. Kwatra, M. Jain, and D. McDuff. Examining the challenges of blood pressure estimation via photoplethysmogram. *Scientific Reports*, 14(1):18318, 2024. 2, 5
- [48] A. Mobiny, P. Yuan, S. K. Moulik, N. Garg, et al. Dropconnect is effective in modeling uncertainty of Bayesian deep networks. *Scientific Reports*, 11(1):5458, 2021. 3
- [49] T. Nair, D. Precup, D. L. Arnold, and T. Arbel. Exploring uncertainty measures in deep networks for multiple sclerosis lesion detection and segmentation. *Medical Image Analysis*, 59:101557, 2020. 3
- [50] R. M. Neal. *Bayesian learning for neural networks*. Springer Science & Business Media, 2012. 3
- [51] S. Oparil and A. P. Miller. Gender and blood pressure. *The Journal of Clinical Hypertension*, 7(5):300–309, 2005. 3
- [52] World Health Organization. World health statistics 2022: monitoring health for the sdgs, sustainable development goals, 2022. 1
- [53] E. O’Brien, J. Petrie, W. Littler, M. De Swiet, et al. The british hypertension society protocol for the evaluation of blood pressure measuring devices. *Journal of Hypertension*, 11(Suppl 2):S43–S62, 1993. 8
- [54] M. F. O’rourke and J. Hashimoto. Mechanical factors in arterial aging: a clinical perspective. *Journal of the American College of Cardiology*, 50(1):1–13, 2007. 2
- [55] J. Park and K. Hong. Robust blood pressure measurement from facial videos in diverse environments. *Heliyon*, 10(4), 2024. 2
- [56] A. Paszke, S. Gross, F. Massa, A. Lerer, et al. PyTorch: An imperative style, high-performance deep learning library. In *Proc. Advances in Neural Information Processing Systems (NeurIPS)*, pages 8024–8035, 2019. 6
- [57] E. Pinto. Blood pressure and ageing. *Postgraduate Medical Journal*, 83(976):109–114, 2007. 3
- [58] M. Poh, D. J. McDuff, and R. W. Picard. Non-contact, automated cardiac pulse measurements using video imaging and blind source separation. *Optics Express*, 18(10):10762–10774, 2010. 2
- [59] M. Rong and K. Li. A blood pressure prediction method based on imaging photoplethysmography in combination with machine learning. *Biomedical Signal Processing and Control*, 64:102328, 2021. 2
- [60] F. Schrumppf, P. Frenzel, C. Aust, G. Osterhoff, et al. Assessment of deep learning based blood pressure prediction from PPG and rPPG signals. In *Proc. IEEE/CVF Conf. Computer Vision and Pattern Recognition Workshop (CVPRW)*, pages 3820–3830, 2021. 2, 3, 5, 6, 7, 1
- [61] G. Slapničar, N. Mlakar, and M. Luštrek. Blood pressure estimation from photoplethysmogram using a spectro-temporal deep neural network. *Sensors*, 19(15):3420, 2019. 1, 4
- [62] I. D. Stephen, V. Hiew, V. Coetzee, B. P. Tiddeman, et al. Facial shape analysis identifies valid cues to aspects of physiological health in caucasian, asian, and african populations. *Frontiers in Psychology*, 8:288503, 2017. 2, 5
- [63] Z. Sun, X. Li, H. Han, J. Tang, et al. The 3rd vision-based remote physiological signal sensing (repss) challenge & workshop. In *CEUR Workshop Proceedings*, 2024. 6

- [64] S. Swati, A. Roy, and E. Ntoutsis. Exploring fusion techniques in multimodal AI-based recruitment: Insights from FairCVdb. *arXiv preprint arXiv:2407.16892*, 2024. 7
- [65] XF Teng and YT Zhang. Continuous and noninvasive estimation of arterial blood pressure using a photoplethysmographic approach. In *Proc. Annual Int. Conf. IEEE Engineering in Medicine and Biology Society (EMBC)*, pages 3153–3156, 2003. 1
- [66] S. Trirongjitmoah, A. Promking, K. Kaewdang, N. Phansiri, et al. Assessing heart rate and blood pressure estimation from image photoplethysmography using a digital blood pressure meter. *Heliyon*, 2024. 2, 6, 1
- [67] M. Valdenegro-Toro. Deep sub-ensembles for fast uncertainty estimation in image classification. *arXiv preprint arXiv:1910.08168*, 2019. 3
- [68] W. Verkruysse, L. O. Svaasand, and J. S. Nelson. Remote plethysmographic imaging using ambient light. *Optics Express*, 16(26):21434–21445, 2008. 2
- [69] W. Wang, A. C. Den Brinker, S. Stuijk, and G. De Haan. Algorithmic principles of remote PPG. *IEEE Transactions on Biomedical Engineering*, 64(7):1479–1491, 2016. 2, 3, 4
- [70] Yeming Wen, Dustin Tran, and Jimmy Ba. BatchEnsemble: an alternative approach to efficient ensemble and life-long learning. In *Proc. Int. Conf. Learning Representations (ICLR)*, 2019. 3
- [71] B. Wu, B. Wu, and C. Hsu. Camera-based blood pressure estimation via windkessel model and waveform features. *IEEE Transactions on Instrumentation and Measurement*, 72:1–13, 2022. 2, 3, 7, 1
- [72] B. Wu, B. Wu, B. Tsai, and C. Hsu. A facial-image-based blood pressure measurement system without calibration. *IEEE Transactions on Instrumentation and Measurement*, 71:1–13, 2022. 2, 3, 5, 6, 7, 1
- [73] B. Wu, L. Chiu, Y. Wu, C. Lai, et al. Contactless blood pressure measurement via remote photoplethysmography with synthetic data generation using generative adversarial networks. *IEEE Journal of Biomedical and Health Informatics*, 2023. 2, 5
- [74] X. Xing and M. Sun. Optical blood pressure estimation with photoplethysmography and FFT-based neural networks. *Biomedical Optics Express*, 7(8):3007–3020, 2016. 1
- [75] S. Yang, J. Sohn, S. Lee, J. Lee, et al. Estimation and validation of arterial blood pressure using photoplethysmogram morphology features in conjunction with pulse arrival time in large open databases. *IEEE Journal of Biomedical and Health Informatics*, 25(4):1018–1030, 2020. 1
- [76] Z. Yu, Y. Shen, J. Shi, H. Zhao, et al. PhysFormer: Facial video-based physiological measurement with temporal difference transformer. In *Proc. IEEE/CVF Conf. Computer Vision and Pattern Recognition (CVPR)*, pages 4186–4196, 2022. 4
- [77] Y. Zhou, H. Ni, Q. Zhang, and Q. Wu. The noninvasive blood pressure measurement based on facial images processing. *IEEE Sensors Journal*, 19(22):10624–10634, 2019. 2, 3, 6, 1

U-FaceBP: Uncertainty-aware Bayesian Ensemble Deep Learning for Face Video-based Blood Pressure Measurement

Supplementary Material

6. Dataset Details

Figure 7 shows the distribution of the subjects’ gender and age in our dataset. There are slightly more males than females, and the number of subjects in their 20s to 60s is similar. Our dataset includes elderly persons in their 70s to 90s.

As mentioned in Sec. 4.1, each subject participated between two and five sets of recordings. One set of them is a BP-raising experiment, and the other sets are static state. In the BP-raising experiment, the subjects placed their feet on a stool and exerted instep strength, as in previous studies [71, 72]. By conducting the BP-raising experiment, we can collect a variety of BP data.

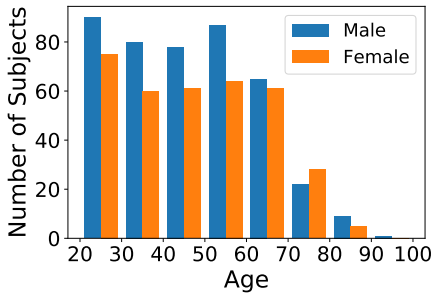


Figure 7. Distribution of subjects’ gender and age in our dataset.

7. Implementation Details

We explain the implementation details of the comparison methods and our U-FaceBP. In order to perform a fair comparison between the methods, we make the implementation such as data preprocessing of the comparison methods and our U-FaceBP as similar as possible. We first explain the common implementation between the methods in Sec. 7.1. We then describe the implementation of the comparison methods in Sec. 7.2 and that of U-FaceBP in Sec. 7.3.

7.1. Common Implementation

As the ROI from face videos, we commonly use the area under the eyes (see Fig. 2 (b)). The methods using PTT-related features, *i.e.*, S-Net, FS-Net, and U-FaceBP use multiple ROIs from the cheek, inner cheek, and forehead (see Fig. 2 (a)). In the comparison methods, we extract rPPG signals using the approaches reported in each paper. The rPPG signal is normalized to mean 0 and standard deviation 1, but a filtering process is not applied to the extracted rPPG signal (we confirm that rPPG signals without filtering generally perform better in BP estimation). The BP values

of the training data are normalized, and the estimated values in the test data are transformed back to the original scale using the mean and standard deviation of the training data. In each epoch, samples of 5 seconds are randomly sampled for model training. The sampling number is 60 for models using rPPG signals, 10 for models using RGB signals (Liu *et al.* [39] and U-FaceBP), and 3 for models using face images (U-FaceBP). The upsampling strategy of training data, number of epochs, optimization algorithm, batch size, and learning rate described in Sec. 4.2 are the same for all methods. Note that the upsampling strategy is not implemented for BP estimation from face images (U-FaceBP) because we confirm that it is not effective. We also implement a scheduler that decreases the learning rate every 10 epochs, in which the rate of decrease is adjusted by monitoring the validation loss.

7.2. Comparison Methods

Mean Regressor is implemented to predict the mean SBP and DBP of the training data in each cross-validation.

Zhou *et al.* [77] used body mass index (BMI) in addition to rPPG signals for BP estimation, but BMI was not acquired in our dataset. Therefore, we use the BMI estimated from the face image (this use is fair for comparison in terms of using only information obtained from the face for BP estimation). Specifically, we use ResNet50 [26] to predict BMI from face images as in a previous method [72], and train a model from ImageNet pre-training weights [14] with the Illinois DOC labeled faces dataset [1]. Then, the method by Zhou *et al.* [77] is implemented to fit the model parameters using the least squares fitting algorithm according to the paper [77].

ResNet1D [60] is implemented with the code in a previous study [25]. AlexNet1D [60] is implemented with reference to the original code [60]. To make a fair comparison with other methods, the model is trained from scratch (not transfer learning as in the above study [60]).

S-Net [72] is implemented according to the paper [72], where models are trained individually for SBP and DBP. Compared to S-Net, FS-Net [72] additionally uses heart rate (HR), heart rate variability (HRV), pulse transit time (PTT), and BMI (from face images). HR and HRV are calculated using rPPG signals from the inner cheek, and PTT is calculated using rPPG signals from the cheek and forehead (see Fig. 2 (a)). BMI is estimated in the same way as in the above implementation of the method by Zhou *et al.* [77].

The method by Trirongjitmoah *et al.* [66] is implemented

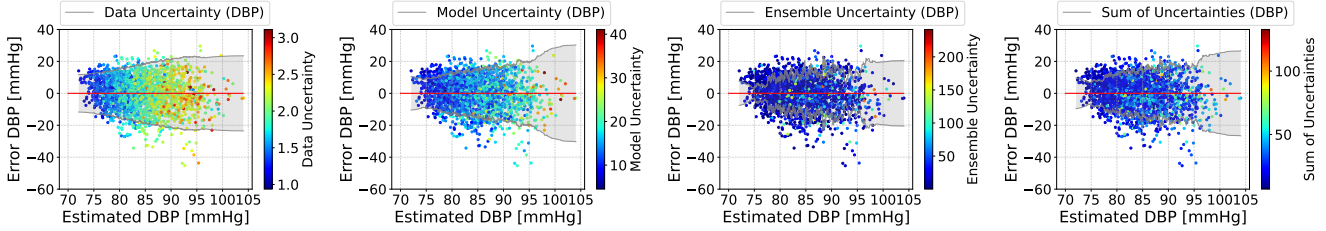


Figure 8. Scatter plots of estimated DBP with U-FaceBP and error of DBP. Four uncertainties are plotted in color, and range of gray lines indicates uncertainty values. Gray lines are smoothed using Savitzky-Golay filter against actual values, and scale is adjusted to figure.

according to the paper [66]. Since the loss function for training is not provided, we use the mean squared error (MSE) loss, which is commonly used for BP estimation.

The method by Liu *et al.* [39] is implemented according to the paper [39]. In terms of computational resources, the number of seeds N in the ensemble method is set to 3, and each frame of face videos is resized to 36×36 .

7.3. U-FaceBP

Most of the implementation for U-FaceBP is explained in Sec. 4.2, but here we describe the other details. The original S-Net [72] seems to train SBP and DBP individually, but our S-Net backbone (rPPG signals) predicts SBP and DBP simultaneously in a single model. MC dropout is implemented in each residual block for S-Net (rPPG signals), each residual block except the first block for ResNet1D (PPG signals), and each residual block for ResNet50 (face images). The dropout probability is 0.2 for S-Net, 0.5 for ResNet1D, and 0.5 for ResNet50. For BP estimation from PPG signals, VPG signals are obtained by the first-order differences of PPG signals, and APG signals are obtained by the first-order differences of VPG signals, according to the implementation by González *et al.* [25].

8. Additional Results

8.1. Uncertainties of DBP

Section 4.5 investigates uncertainties of SBP, but this section investigates uncertainties of DBP. Figure 8 shows the relationship between estimated DBP with U-FaceBP and the error of DBP. As in Fig. 5, the data, model, ensemble, and sum of uncertainties are illustrated, where the uncertainty is higher when the gray line is wider. Overall, each uncertainty of DBP shows the same tendency as that of SBP discussed in Sec. 4.5. Although the data uncertainty tends to be larger when the estimated DBP is higher, the increase in uncertainty is smaller than for SBP. This may be because the range of hypertension in DBP is narrow (90 to 139 mmHg in our dataset) and the regression task in hypertension is easier than in SBP. Figure 9 shows the relationship between uncertainties and estimation performance for DBP. The MAE is smaller when the data, model, and sum of uncertainties are

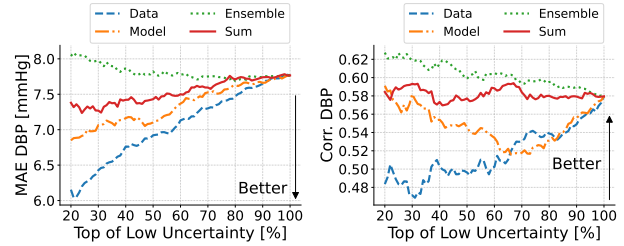


Figure 9. Relationship between top of low uncertainty (top $x\%$ of predictions when predictions are ranked in ascending order of uncertainties) and their MAE and correlation coefficient for DBP.

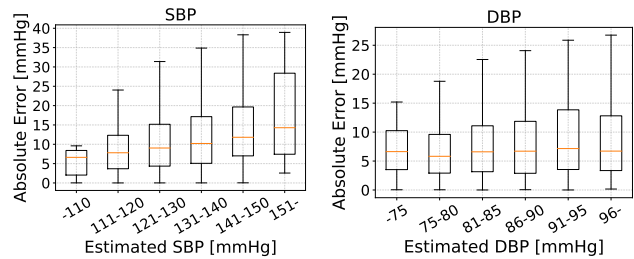


Figure 10. Box plot of absolute error against estimated BP.

lower, indicating that lower those uncertainties lead to better performance. On the other hand, in terms of the correlation coefficient, the ensemble and sum of uncertainties perform well (the model uncertainty performs only partially well). Considering overall the results of the SBP (Fig. 6) and DBP (Fig. 9), we conclude that the sum of uncertainties is reasonable as prediction confidence.

From the results of the uncertainties of SBP (Fig. 5) and DBP (Fig. 8), we confirm that the uncertainties tend to increase when the estimated BP is higher. Figure 10 shows the box plot of the absolute error (AE) against the estimated BP. Note that outliers are removed from the box plots. The SBP box plot indicates that the median and range of AE increase when the estimated SBP is higher. The DBP box plot indicates that the median of AE is comparable but the range of AE increases when the estimated DBP is higher. These results show that AE increases or becomes more dispersed when the estimated BP is higher. Therefore, it is reasonable that the uncertainties increase for higher estimated BP.

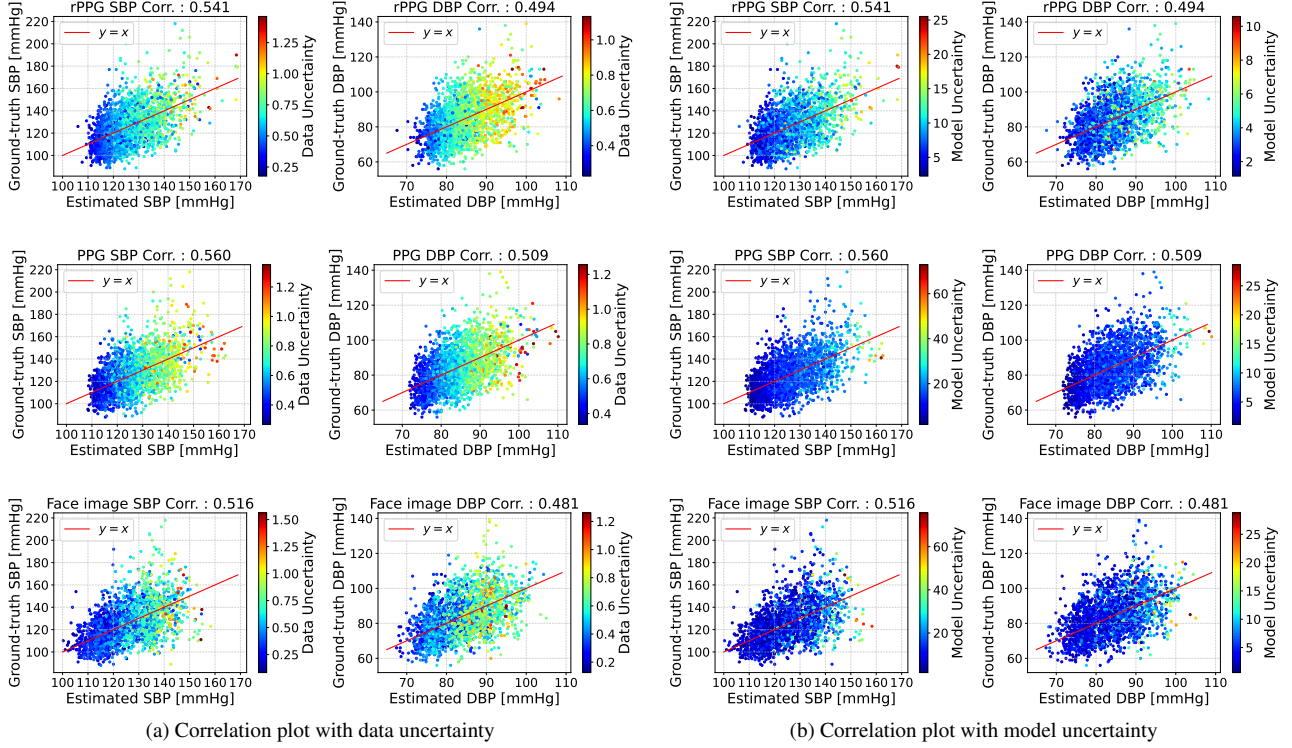


Figure 11. Correlation plot of each ensemble component with (a) data and (b) model uncertainties. First, second, and third rows correspond to BP estimation from rPPG, PPG signals, and face images, respectively. For example, first row corresponds to $U_{\text{rppg, sbp}}^{\text{data}}$, $U_{\text{rppg, dbp}}^{\text{data}}$, $U_{\text{rppg, sbp}}^{\text{model}}$, and $U_{\text{rppg, dbp}}^{\text{model}}$ from left to right.

8.2. Uncertainties of Ensemble Components

In Secs. 4.5 and 8.1, we investigate the data and model uncertainties derived from the sum of all ensemble components, *i.e.*, $U_{\text{rppg, sbp}}^{\text{data}} + U_{\text{ppg, sbp}}^{\text{data}} + U_{\text{img, sbp}}^{\text{data}}$ for data uncertainty and $U_{\text{rppg, sbp}}^{\text{model}} + U_{\text{ppg, sbp}}^{\text{model}} + U_{\text{img, sbp}}^{\text{model}}$ for model uncertainty. Figure 11 shows the correlation plot of each ensemble component with the data and model uncertainties (*e.g.*, the first row corresponds to $U_{\text{rppg, sbp}}^{\text{data}}$, $U_{\text{rppg, dbp}}^{\text{data}}$, $U_{\text{rppg, sbp}}^{\text{model}}$, and $U_{\text{rppg, dbp}}^{\text{model}}$ from the left to right). As with the results in Secs. 4.5 and 8.1, the uncertainties tend to increase when the estimated BP is higher. On the other hand, there are also predictions with low uncertainty even when the estimated BP is high (*e.g.*, data uncertainty in BP estimation from PPG signals).

From the correlation plots, it can be seen that BP estimation from rPPG or PPG signals sometimes correctly predicts considerably high BPs (SBP above 160 mmHg and DBP above 105 mmHg). This suggests that the PTT and pulse waveform provide features associated with severe hypertension. On the other hand, BP estimation from face images correctly predicts considerably low BPs (SBP below 110 mmHg and DBP below 70 mmHg). This suggests that facial appearance can be used to identify persons with low BP (especially young females, see Sec. 8.3 for the details).

8.3. Relationship Between Age, Gender, and BP

BP is closely related to a person’s age [57] and gender [51]. Here, we discuss our BP estimation results in terms of age and gender. Figure 12 (a) shows the box plot of the ground-truth BP against age and gender in our dataset (outliers are removed from the box plot). Figure 12 (b) shows the variance of the ground-truth BP against age and gender. From the box plot, we can see that SBP increases continuously as age increases. On the other hand, DBP increases from the 20s to the 60s, and then slowly decreases until the 80s. This is a typical case of isolated systolic hypertension, and this tendency in our dataset is consistent with previous studies [57]. BP is lower in females than in males during younger ages, but becomes comparable after their 50s, which is also generally consistent with previous studies [51]. The variance of BP increases continuously from the 20s to the 70s, and then decreases until the 80s. Therefore, we can see that BP is more diverse in elderly persons than in young persons.

Figure 13 (a) shows the box plot of the estimated BP against age and gender for each ensemble component (outliers are removed from the box plot). Figure 13 (b) shows the box plot of the data uncertainty against age and gender (outliers are removed from the box plot). Here, we

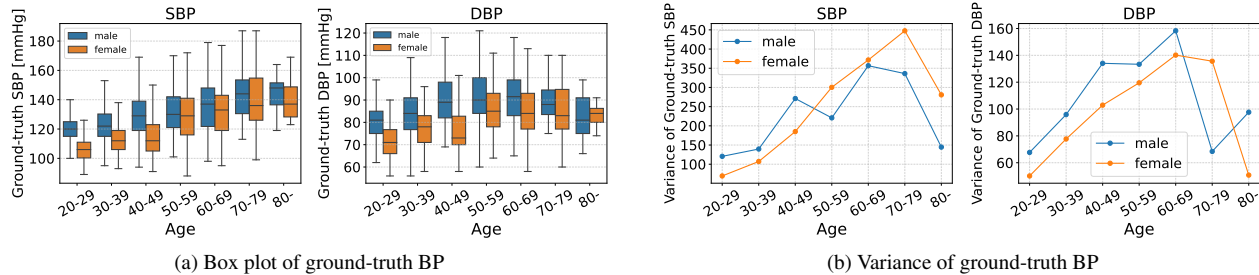


Figure 12. (a) Box plot and (b) variances of ground-truth BP against age and gender. From left to right, box plots of ground-truth SBP and DBP and variances of ground-truth SBP and DBP against age and gender.

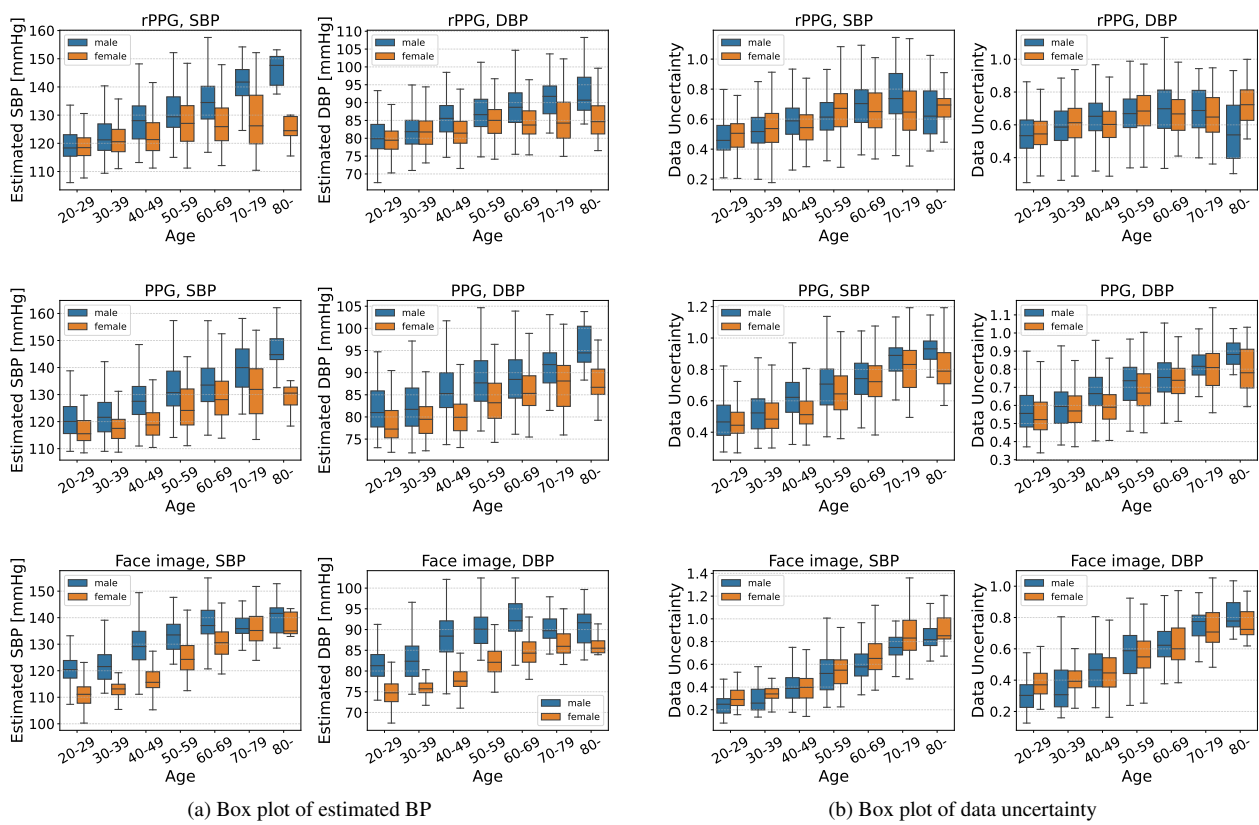


Figure 13. Box plots of (a) estimated BP and (b) data uncertainty against age and gender for each ensemble component. First, second, and third rows correspond to BP estimation from rPPG, PPG signals, and face images, respectively. For example, first row corresponds to box plots of estimated SBP and DBP and box plots of data uncertainty of SBP and DBP against age and gender in BP estimation from rPPG signals, from left to right.

select data uncertainty to reveal the uncertainty of the BP estimation task. The box plots of the estimated BP show that all ensemble components tend to estimate higher BP as age increases. These results suggest that the rPPG and PPG signals capture “vascular aging”, specifically focusing on changes in PTT [16] and pulse waveform [5] associated with aging. The face images capture “facial aging” and successfully capture the relationship between age, gender, and

BP (e.g., decline in DBP after the 60s, BP differences between the genders). Table 3 shows that BP estimation from rPPG or PPG signals is slightly better than that from face images, suggesting that capturing “vascular aging” is more effective than capturing “facial aging” for BP estimation. Ultimately, Table 3 indicates that the ensemble method that captures both types of aging is the most effective. Interestingly, the box plots of data uncertainty in Fig. 13 (b) show

that the uncertainty increases with age. This result may be related to the fact that the variance of BP increases with age (see Fig. 12 (b)), making BP estimation more difficult. In particular, the change in data uncertainty with age in BP estimation from rPPG signals is similar to the change in BP variance (*i.e.*, the values increase from the 20s to the 70s, and then decrease until the 80s).